

Figure 1. Representative multistep semisynthesis of paclitaxel (R = variable phenyl analogues, heteroaromatics, and alkyl derivatives): (i) (a) Et_3SiCl , pyridine; (b) acetyl chloride, pyridine; (ii) (a) *n*-butyllithium, compound A; (b) HF, pyridine. Proposed biosynthesis of paclitaxel (and its analogues): (iii) 10-deacetylbaccatin III acetyltransferase, acetyl CoA; (iv) 13-*O*-phenylpropanoyltransferase, an isoserinyl CoA (27); (v) *N*-debenzoyltaxane-*N*-benzoyltransferase, benzoyl CoA. Structure designations: 10-deacetylbaccatin III (1), 7-*O*-triethylsilylbaccatin III (2), paclitaxel (R = phenyl) (or an analogue) (3), baccatin III (4), and *N*-debenzoylpaclitaxel (R = phenyl) (or an analogue) (5).

paclitaxel results in an inactive *N*-debenzoyl-2'-deoxy paclitaxel.²⁵

Various semisynthesized second-generation paclitaxel with a modified isoserinyl side chain includes, for example, addition of an *m*-hydroxyl on the phenylisoserinyl ring (8) (Table 1) that allows construction of a conformationally constrained analogue with improved binding to its β -tubulin target.²⁶ Another bioassay showed that a *p*-fluoro analogue (10) had a potency (IC_{50}) ~20-fold greater than that of docetaxel against multiple drug-resistant human leukemia cells.²⁷ In addition, pyridyl analogues (16 and 17)^{16,17} were found to be more potent than paclitaxel or docetaxel in vincristine-resistant cancer cell lines expressing P-glycoprotein drug-efflux pumps. Fluoro-pyridyl compound tasetaxel (18), in phase I clinical trials, is an oral taxane used as a single agent or in combination with the antineoplastic pharmaceutical Xeloda (Genentech; generic name capecitabine) in patients with solid tumors.²⁸ Simotaxel (12) was developed as a more potent analogue by replacement of the phenylisoserinyl group with a polar thienylisoserinyl group for oral bioavailability.²⁹ Phase I clinical trials with 12, however, were terminated for undisclosed reasons.³⁰ It should be noted that several taxoids that stalled in clinical trials for “undisclosed reasons” are not cited for drug failure (clinicaltrials.gov). It is perceived that the cost of screening efficacious new taxoid compounds in a slow economy has forced pharmaceutical companies to curtail development of new drug analogues.³¹ Driven by economics only, these

companies refocus research efforts on previously approved drugs, thus likely reducing the number of new taxoids brought to market.

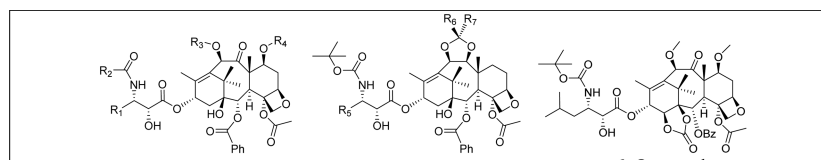
Other alkyl/alkenylisoserine taxoids include the cyclohexylisoserine analogue 13, which has activity superior to that of paclitaxel in a microtubule disassembly inhibition assay and is cytotoxic against a doxorubicin-resistant murine leukemia cell line (P388/Dox).³² Ortataxel (6) (Spectrum Pharmaceuticals), with an isobutyl substituent on the isoserinyl moiety,³³ was last known to be in phase II clinical trials³⁴ showing activity against paclitaxel- and docetaxel-resistant breast and non-small cell lung cancers.³³

During the mid-1990s to early 2000s when these paclitaxel analogues were semisynthesized, there was little advancement of the biosynthesis of the natural product paclitaxel or its nonnatural analogues from baccatin III. Limitations against developing a biosynthetic approach were largely caused by a lack of identified paclitaxel genes from which a biocatalytic platform could be built.³⁵ The first few enzymes identified on the paclitaxel pathway in *Taxus* plants were a cyclase, a few hydroxylases, and five acyl CoA-dependent acyltransferases.⁸ None of the CoA ligases needed to make key acyl CoA intermediates had been identified, and this omission provided motivation for our earlier study.⁶ We repurposed a tridomain TycA (Phe-ATE), on a nonribosomal peptide synthetase pathway, as a CoA ligase³⁶ to convert phenylisoserine to phenylisoserinyl CoA, a linchpin pathway intermediate. Encouraged by this finding, we used a truncated Phe-AT didomain in this study to biosynthesize other isoserinyl CoA analogues. The selection of the isoserine substrates synthesized herein for our biosynthetic study was based in part on the various isoserine variants found in bioactive paclitaxel analogues semisynthesized in previous studies (Table 1). The biocatalyzed CoA thioesters can potentially be incorporated into a semibiosynthetic scheme to make not only paclitaxel from baccatin III but also various precursors toward paclitaxel analogues, some of which are in clinical trials.^{11,35,37–39} In addition, the scope of this document covers the stereospecificity of Phe-AT for racemic isoserines and evaluates how a single variable that changes steric and/or electronic properties of monosubstituted arylisoserines affects the turnover rate of the catalyst.

MATERIALS AND EXPERIMENTAL DETAILS

Expression, Purification, and Characterization of Phe-AT Proteins. Plasmids pET28phe-at and pET28phe-atS563A (see the Supporting Information) were separately used to transform *Escherichia coli* BL21(DE3) cells. Five 10-mL cultures of the two *E. coli* transformants were separately grown in LB medium supplemented with 50 $\mu\text{g mL}^{-1}$ kanamycin at 37 °C for 12 h. A 10-mL aliquot of each seed culture expressing Phe-AT/His and Phe-AT(S563A)/His was used to inoculate LB medium (5 \times 1 L for each transformant). The bacteria were grown at 37 °C to an OD_{600} of ~0.6; then isopropyl β -D-1-thiogalactopyranoside was added to a final concentration of 0.5 mM, and the culture was grown for 18 h at 16 °C. The cells were pelleted by centrifugation (30 min at 4000g) at 4 °C, resuspended in binding buffer [20 mM Tris-HCl buffer containing 0.5 M NaCl and 5 mM imidazole (pH 7.8)], lysed by sonication, and then centrifuged at 15000g for 0.5 h. The supernatant was decanted and centrifuged at 135000g for 1.5 h to remove cell wall debris and light membranes.

Table 1. Examples of Paclitaxel, Docetaxel, and Various Modified Analogues



Drug	R ₁	R ₂	R ₃	R ₄	R ₅	R ₆	R ₇
3 Paclitaxel	 (a)	a	 (c)	H	---	---	---
7 Docetaxel	a	 (b)	H	H	---	---	---
8		a	c	H	---	---	---
9		a	c	H	---	---	---
10			H	H	---	---	---
11 Milataxel		b	H		---	---	---
12 Simotaxel				H	---	---	---
13		b	H	H	---	---	---
14		b	 (d)	H	---	---	---
15 SB-T-1214		b	 (d)	H	---	---	---
16	---	---	---	---			H
17	---	---	---	---		CH ₃	CH ₃
18 Tetasetaxel	---	---	---	---			H

Crude soluble protein isolated from bacteria expressing Phe-AT/His and Phe-AT(S563A)/His was estimated by the Bradford protein assay at ~50 and ~75 mg of total protein, respectively. These fractions were independently loaded onto a Ni-NTA affinity column (Qiagen, Valencia, CA) and eluted according to the protocol described by the manufacturer. The column was eluted with an increasing concentration of imidazole (from 20 to 250 mM) in binding buffer. Fractions containing the His-tagged enzymes were identified by sodium dodecyl sulfate–polyacrylamide gel electrophoresis (SDS–PAGE) analysis and Coomassie Blue staining. Fractions eluting in 50–100 mM imidazole were combined and showed >95% pure protein corresponding to a molecular weight consistent with that of the calculated molecular weight for Phe-AT/His and Phe-AT(S563A)/His at 69.6 kDa. Each enzyme solution (100 mL) was separately concentrated to 1 mL by size-selective centrifugation (Centriprep 30000 MWCO unit, Millipore, Billerica, MA). The buffer was exchanged with assay buffer [50 mM HEPES containing 100 mM NaCl and 1 mM EDTA (pH 8.0)] over five dilution/concentration cycles. Enzyme purity was estimated by SDS–PAGE with Coomassie Blue staining. The purified proteins were stored at –80 °C. The concentration of each protein [35 and 28 mg/mL for Phe-AT and Phe-AT(S563A), respectively] was determined on a NanoDrop ND1000 spectrophotometer (Thermo Scientific, Wilmington, DE). The estimated extinction coefficient (ϵ_{280}) of Phe-AT and Phe-AT(S563A) was set at 71740 M⁻¹ cm⁻¹, based on the approximation that spectral contributions of the

tyrosine, tryptophan, and cysteine at A₂₈₀ do not differ significantly in the native protein and the denatured form.^{61,62}

Kinetic Evaluation of Phe-AT and Phe-AT(S563A) for CoA and Amino Phenylpropanoids. (*R*)- β -Phenylalanine and (*2R,3S*)-phenylisoserine (each at 1 mM) were separately incubated in 1-mL reaction mixtures containing 100 mM HEPES (pH 8.0), ATP (1 mM), MgCl₂ (3 mM), CoA (1 mM), and Phe-AT or Phe-AT(S563A) (100 μ g) to establish steady-state conditions with respect to protein concentration and time at 31 °C. Under steady-state conditions, (*R*)- β -phenylalanine and (*2R,3S*)-phenylisoserine at 5–2000 μ M were separately incubated with Phe-AT and Phe-AT(S563A) (20 μ g) for 15 min. The assays were quenched by acidifying to pH ~2 (10% formic acid). Acetyl CoA (1 μ M) was added as an internal standard to each sample to correct for losses during workup. The biosynthetic products were quantified by liquid chromatography electrospray multiple-reaction monitoring (LC–ESI-MRM) mass spectrometry on a Quattro-Premier XE mass spectrometer coupled to an Acquity UPLC system fitted with a C18 Ascentis Express column (2.5 mm \times 50 mm, 2.7 μ m) at 30 °C. An aliquot (5 μ L) of each sample was loaded onto the column, and the analytes were eluted with a solvent gradient of acetonitrile (solvent A) and 0.05% triethylamine in distilled water (solvent B) (held at 2.5% solvent A for 3.17 min, increased to 100% solvent A over 5 s with a 2 min hold, and then returned to 2.5% solvent A over 5 s with a 50-s hold) at a flow rate of 0.4 mL/min. The effluent from the column was directed to the mass spectrometer where the first quadrupole mass analyzer (in negative ion mode) was set to select for the

Table 2. Synthesis of Isoleucine Analogues

$R_1 =$	22a	22b	22c	22d	22e	22f	22g
	22a						
	(37) (80) (78) (23) ^b	(41) (81) (98) (33)	(51) (67) (98) (33)	(40) (78) (81) (25)	(80) (63) (98) (49)	(47) (81) (84) (32)	(84) (69) (84) (49)
	22h	22i	22j	22k	22l	22m	22n
	(59) (42) (98) (24)	(33) (70) (98) (23)	(95) (95) (100) (90)	(75) (52) (95) (37)	(81) (41) (95) (32)	(51) (87) (95) (42)	(84) (88) (98) (72)
	22o	22p	22q	22r	22s	22t	22u
	(66) (81) (98) (52)	(94) (95) (98) (88)	(47) (61) (97) (28)	(25) (56) (96) (13)	(79) (55) (95) (41)	(79) (50) (98) (39)	(82) (54) (98) (43)
	22v	22w	22x	22y	22z	22aa	22bb
	(18) (84) (15) ^c	(26) (94) (24)	(12) (72) (9)	(8) (98) (65) (5)	(35) (66) (95) (22)	(9) (72) (65) (4)	(70) (85) (98) (58)

^a(i) (a) Dichloromethane, 4 Å molecular sieves, 12 h, 23 °C; (b) triethylamine, acetoxyacetyl chloride, dichloromethane, 0–23 °C, 2–5 h; (ii) (a) ceric ammonium nitrate in H₂O, acetonitrile, 0 °C, 1–3 h (up to this step, X = acetyl in **22t** and **22u**); (b) 7 N HCl, reflux, 24 h (after this step, X = H in **22t** and **22u**). ^bThe entries in parentheses in groups of four are the percent isolated yield after steps *i*-a and *i*-b, the percent isolated yield after step *ii*-a, the percent isolated yield after step *ii*-b, and the overall percent yield of the isoleucine product with respect to the aldehyde (bold) from left to right, respectively. ^cThe entries in parentheses in groups of three for compounds **22v**, **22w**, and **22x** are the percent isolated yield after step *i*-b in Figure 2, the percent isolated yield after step *ii*-b in Figure 2, and the overall percent yield of the pyridylisoleucine product with respect to the aldehyde (bold) from left to right, respectively.

molecular ion of a biosynthesized acyl CoA product. The selected ion was then directed to a collision gas chamber wherein the collision energy was optimized to maximize the abundance of a signature fragment ion (m/z 408.31, derived by a fragmentation reaction in the CoA moiety of the acyl CoA) monitored in the second quadrupole mass analyzer in negative ion mode. The peak area under the curve of the monitored fragment ion at m/z 408.31 corresponding to each biosynthetic phenylpropionyl CoA thioester was converted to concentration by comparison to a standard curve of authentic CoA (0.048–100 μ M). The initial velocity (v_0) of production of (*R*)- β -phenylalanyl and (2*R*,3*S*)-phenylisoserinyl CoA made in separate enzyme catalysis assays was plotted against substrate concentration and fit by nonlinear regression to the Michaelis–Menten equation (R^2 was typically between 0.90 and 0.99) to calculate the apparent K_M and k_{cat} (see Figure S40).

The apparent K_M values of Phe-AT and Phe-AT(S563A) for CoA were assessed by incubating each enzyme separately with (*R*)- β -phenylalanine (1 mM), MgCl₂ (3 mM), ATP (1 mM), and CoA (5–2000 μ M) at 31 °C for 15 min. Acetyl CoA (1 μ M) was added as an internal standard to each sample. The products of the enzyme-catalyzed reactions were quantified by LC–MRM mass spectrometry, and the monitored fragment ion (m/z 408.31) derived from the CoA thioester analytes in the effluent was quantified in a manner identical to the procedure described previously.⁶ The initial velocity (v_0) of production of (*R*)- β -phenylalanyl CoA made in separate assays was plotted against substrate concentration and fit by nonlinear regression to the Michaelis–Menten equation (R^2 was 0.9) to calculate K_M .

Kinetic Evaluation of Phe-AT for CoA and Phenylisoleucine Stereoisomers. The apparent kinetic parameters of Phe-AT for (2*R*,3*R*)-phenylisoleucine were determined to provide a basis of comparison against the catalytically active (2*R*,3*S*)-phenylisoleucine isomer. (2*R*,3*R*)-Phenylisoleucine (at 1 mM) was incubated in a 1 mL reaction mixture containing 100 mM HEPES (pH 8.0), ATP (1 mM), MgCl₂ (3 mM), CoA (1 mM), and Phe-AT (100 μ g) to establish steady-state conditions with respect to protein concentration and time at 31 °C. Aliquots (100 μ L) were taken at various time points between 0 and 2 h and their reactions quenched with 10% formic acid (5 μ L). Acetyl CoA (1 μ M) was added as the internal standard, and the samples were analyzed as described above. The kinetic assays with (2*R*,3*R*)-phenylisoleucine were performed in a manner similar to the procedure described for (2*R*,3*S*)-phenylisoleucine. The resulting (2*R*,3*R*)-phenylisoleucinyl CoA biosynthetic product was analyzed by the LC–ESI-MRM method used before. The peak area under the curve of the monitored fragment ion at m/z 408.31 derived from a molecular ion consistent with that of biosynthetic (2*R*,3*R*)-phenylisoleucinyl CoA was converted to concentration by comparison to a standard curve of authentic CoA (0.048–100 μ M). The initial velocity (v_0) of production of (2*R*,3*R*)-phenylisoleucinyl CoA made in separate assays was plotted versus substrate concentration and fit by nonlinear regression to the Michaelis–Menten equation (R^2 was typically between 0.90 and 0.99) to calculate the apparent K_M and k_{cat} .

Activity Assay for the Determination of the Substrate Specificity of Phe-AT. To identify productive isoleucine substrates, each isoleucine (2 mM) was incubated separately

with CoA (1 mM), ATP (1 mM), MgCl₂ (3 mM), and purified Phe-AT enzyme (1 mg) in 100 mM HEPES (pH 8.0) in a 1 mL reaction mixture. The reaction mixtures were incubated for 8 h at 31 °C. Aliquots (100 μL) were withdrawn initially at 10, 20, and 40 min and then at 1, 2, 4, 6, and 8 h and transferred to 96-well plates, the reactions quenched immediately with 10% formic acid (20 μL), and the samples analyzed on the LC-Quattro-Premier XE mass spectrometer as described above. An aliquot (5 μL) of each sample was loaded onto the column, and the analytes were eluted with a solvent gradient of acetonitrile (solvent A) and 0.05% triethylamine in distilled water (solvent B) (held at 2.5% solvent A for 3.17 min, increased to 100% solvent A over 5 s with a 2-min hold, and then returned to 2.5% solvent A over 5 s with a 50-s hold) at a flow rate of 0.3 mL/min.

Apparent Rates of Phe-AT with the Isoleucine Substrates. The conversion rate of Phe-AT for thioesterification of the isoleucine analogues to their isoleucinyl CoA thioesters was determined by incubating each isoleucine (2 mM) separately with ATP (1 mM), CoA (1 mM), MgCl₂ (3 mM), and purified Phe-AT enzyme (1 mg) in 100 mM HEPES (pH 8.0) at 31 °C for 2 h in triplicate. Time course assays performed using Phe-AT (1 mg) with the isoleucine substrates provided a justification for the estimation of the relative rates to be at steady state at 2 h. At the end of each reaction, acetyl CoA (1 μM) was added as the internal standard to each sample to correct for losses during workup. The biosynthetic thioester products were quantified by liquid chromatography–multiple-reaction monitoring (MRM) mass spectrometry on a Quattro-Premier XE mass spectrometer with an elution gradient as described above. The peak area of the monitored fragment ion at *m/z* 408.31 corresponding to each biosynthetic isoleucinyl CoA thioester was converted to concentration by comparing the peak area of the same ion generated by authentic CoA using linear regression analysis.

RESULTS AND DISCUSSION

Synthesis of Isoleucine Analogues. Several methods for the synthesis of phenylisoleucine analogues proceed through reactions involving asymmetric epoxidation,³⁷ dihydroxylation,³⁸ chemoenzymatic resolution,³⁹ aminohydroxylation, or the conrotatory Staudinger [2+2] cycloaddition of an imine and ketene that makes a key β-lactam intermediate.^{30,31} We used the latter electrocyclic cycloaddition reaction with readily available reagents for the synthesis of racemic phenylisoleucine analogues substituted with *ortho*-(F, Cl, Br, CH₃, OCH₃, NO₂), *para*-(F, Cl, Br, CH₃, OH, OCH₃, NO₂), or *meta*-(F, Cl, Br, CH₃, OH, OCH₃, NO₂) (Table 2). This procedure was also used to make β-(thiophenyl)isoleucine and various β-(alkyl)-isoleucines. Following a previously described procedure,⁴⁰ we reacted benzaldehyde analogues with *p*-anisidine to form a Schiff base. In a one-pot sequence, the Schiff base reacted with acetoxyacetyl chloride and triethylamine to form the *cis*-β-lactam racemate. Oxidation with ceric ammonium nitrate removed the *p*-methoxyphenol group to afford the *N*-deacetylated β-lactam. Reflux in 7 N HCl hydrolyzed the *O*-acetyl group and converted the lactam ring to the isoleucines in a single step (Table 2). Incorporating an early one-pot reaction sequence and accomplishing the ester hydrolysis and ring opening in a single step shortened the previously described synthesis of isoleucine racemates from five to three steps.⁴⁰ The overall yields of these arylisoleucines ranged from 4% (22aa) to 90% (22j). Because each Schiff base was isolated by an identical

procedure, differences in isolated yield likely resulted from the electronic effects of the substituent on the aryl ring. The substituent effects from the aryl aldehyde had a significant effect on the overall yield of the lactam. Aryl aldehydes with electron-withdrawing substituents (*m*-halogen, *o*- and *p*-fluoro, or NO₂) or no substituent, and branched alkyl aldehydes, generally yielded 9–47% of the lactam in the one-pot reaction (Table 2), far lower than the average (~58%) isolated yield for this step. To contrast, aryl aldehydes with moderate to strong electron-donating substituents (methyl, methoxy, and acetoxy) typically yielded 51–95% of the lactam. These observations suggested that electron-donating substituents stabilized either the electrophilic carbon in the imine reaction, the cycloaddition reaction, or both, priming them for effective nucleophilic attack. Oxidative removal of the anisole protecting group in the next step averaged an ~71% yield for 25 *N*-dearylation reactions described herein, and the electronics of the substituent did not seemingly influence the yields. The hydrolysis step with 7 N HCl to liberate the isoleucine-HCl salt was generally quantitative, giving on average an ~92% isolated yield relative to the lactam (Table 2).

The β-(pyridyl)isoleucines were synthesized with modifications of the method used to make the substituted phenylisoleucines (Figure 2). To form the pyridyl-substituted lactam

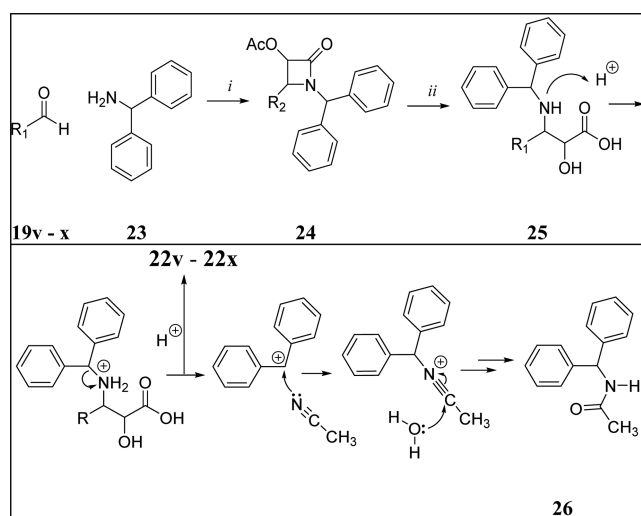


Figure 2. Synthesis of pyridylisoleucine isomers: (i) (a) dichloromethane, 4 Å molecular sieves, 12 h, 23 °C; (b) triethylamine, acetoxyacetyl chloride, dichloromethane, 0 °C, 3 h; (ii) acetonitrile, 7 N HCl, reflux, 24 h.

rings (22v, 22w, and 22x) through the Staudinger reaction, benzhydrylamine was used instead of *p*-anisidine because oxidative removal of the anisole with ceric ammonium nitrate in the presence of the pyridyl ring prevented the *N*-deprotected lactam products from forming. Likely, the pyridyl rings dimerized through a radical cation mechanism on treatment with ceric ammonium nitrate, similar to the mechanism of dimerization for 2-(furan-3-yl)pyrroles mediated by ammonium cerium(IV) nitrate described in an earlier study.⁴¹ After making the benzhydryl lactams, we proposed a two-step sequence of acid hydrolysis to open the lactam ring and remove the *O*-acetyl group, followed by hydrogenolysis to eliminate the benzhydryl moiety. Surprisingly, reflux of the protected lactam under acidic conditions made the β-(pyridyl)isoleucines directly, and the hydrogenolysis step was unnecessary (Figure 2). The

Table 3. Steady-State Kinetic Parameters of TycA Variants

	Phe-AT	Phe-ATE ^a (R)- β -Phe	Phe-AT(S563A)	Phe-ATE(S563A) ^a
$k_{\text{cat}}^{\text{app}}$ (min ⁻¹)	14.6 ± 0.5	1.6 ± 0.3	22.0 ± 4.1	3.0 ± 0.04
K_{M} (μM)	46 ± 3	51 ± 8	33 ± 5	62 ± 1
$k_{\text{cat}}^{\text{app}}/K_{\text{M}}$ (s ⁻¹ M ⁻¹)	5308 ± 119	527 ± 129	11200 ± 500	803 ± 17
		(2R,3S)-PheIso		
$k_{\text{cat}}^{\text{app}}$ (min ⁻¹)	1.5 ± 0.2	0.25 ± 0.02	1.1 ± 0.7	0.43 ± 0.01
K_{M} (μM)	440 ± 62	89 ± 15	327 ± 106	190 ± 10
$k_{\text{cat}}^{\text{app}}/K_{\text{M}}$ (s ⁻¹ M ⁻¹)	57.4 ± 1.7	46.7 ± 8.7	53.3 ± 16.7	37.5 ± 2.1
		CoA ^b		
$k_{\text{cat}}^{\text{app}}$ (min ⁻¹)	10 ± 2	0.75 ± 0.05	29 ± 8	0.9 ± 0.08
K_{M} (μM)	208 ± 57	2000 ± 200	562 ± 149	804 ± 26
$k_{\text{cat}}^{\text{app}}/K_{\text{M}}$ (s ⁻¹ M ⁻¹)	838 ± 74	6.3 ± 0.7	853 ± 198	18.7 ± 1.8
		(2R,3R)-PheIso		
$k_{\text{cat}}^{\text{app}}$ (min ⁻¹)	0.78 ± 0.13			
K_{M} (μM)	380 ± 70			
		(2S,3R)-PheIso		
$k_{\text{cat}}^{\text{app}}$ (min ⁻¹)	nd ^c			
K_{M} (μM)	nd ^c			

^aData from ref 6. ^bKinetic measurements for CoA were taken in the presence of (R)- β -phenylalanine, ATP, and MgCl₂ at apparent steady state. All values are expressed as means ± standard deviations of triplicate results. ^cCoA thioester product was below the LC–ESI-MS detection limit.

benzhydrylacetamide byproduct made in the reaction suggested an S_N1 mechanism that released a benzhydryl carbocationic intermediate, which was captured by the acetonitrile solvent. Subsequent acid hydrolysis of the acetonitrile moiety produced the amide byproduct as confirmed by ¹H nuclear magnetic resonance (NMR) and LC–ESI-MS analysis (Figures S38 and S39, respectively).

Construction and Expression of Phe-AT and Phe-AT(S563A). An earlier study showed that the wild-type *tycA* cDNA encoding the adenylation, thiolation, and epimerization domains (Phe-ATE) functioned as a CoA ligase with β -amino β -phenylpropanoates.⁶ Here, Phe-ATE was truncated to encode only the adenylation and thiolation domains (Phe-AT) and thus eliminate recombinant expression of the 400-amino acid epimerization domain. As important was the fact that the possibility of epimerization of aminoacyl CoA products was eliminated. In addition, a Phe-AT(S563A) mutant derived from Phe-AT was expressed without S563, which was done with Phe-ATE in an earlier study.⁶ This mutation prevented natural *O*-phosphopantetheinylation of Ser563 of the enzyme and thus also abrogated subsequent enzyme-linked thioesterification of the phenylpropanoate substrates in the *E. coli* expression host. The solubly-expressed enzymes Phe-AT and Phe-AT(S563A) were isolated from bacterial lysates and purified by Ni-affinity chromatography for use in the CoA ligase activity assays.

Activity and Kinetic Analyses of Phe-AT. The activities of Phe-AT and Phe-AT(S563A) were compared to those of the corresponding tridomain cognates of Phe-ATE measured in an earlier study.⁶ Phe-AT and its mutant were incubated with CoA, Mg²⁺, ATP, and separately with substrates (R)- β -phenylalanine and (2R,3S)-phenylisoserine. (R)- β -Phenylalanine was the superior phenylpropanoid substrate of Phe-ATE in an earlier study⁶ and thus was used here to help benchmark the activity of the Phe-AT mutants. The identity of the biosynthetic thioester products was verified by LC–ESI-MS/MS and comparison against mass fragmentation profiles of authentic amino acyl CoA thioesters. An LC–ESI/MS/MS technique was used to quantify the biosynthetic products for kinetic analysis.

Phe-AT and Phe-AT(S563A) were faster than the wild-type Phe-ATE in turning over the two test substrates (Table 3). The apparent k_{cat} ($k_{\text{cat}}^{\text{app}}$) of Phe-AT for (R)- β -phenylalanine was improved 7-fold compared to that of Phe-ATE, whereas the K_{M} values of truncated and wild-type catalysts were virtually of the same order of magnitude. Similarly, Phe-AT (6-fold increase) and Phe-AT(S563A) (2.5-fold increase) were faster than Phe-ATE and Phe-ATE(S563A), respectively, at turning over (2R,3S)-phenylisoserine to its CoA thioester.

The $k_{\text{cat}}^{\text{app}}$ of Phe-AT(S563A) for CoA was 32-fold higher compared to that of its wild-type counterpart, Phe-ATE(S563A), while the $k_{\text{cat}}^{\text{app}}$ of Phe-AT for CoA improved 13-fold versus that of Phe-ATE. The catalytic efficiency ($k_{\text{cat}}^{\text{app}}/K_{\text{M}}$) of Phe-AT for CoA improved 2 orders of magnitude over that of Phe-ATE due mainly to a lower K_{M} value. Phe-AT and Phe-AT(S563A) also had catalytic efficiencies for (R)- β -phenylalanine increased 10- and 14-fold, respectively, versus those of their ATE counterparts due mainly to a 7-fold increase in the $k_{\text{cat}}^{\text{app}}$ values of both catalysts. It was interesting to find that the catalytic efficiencies of Phe-AT and Phe-AT(S563A) for (2R,3S)-phenylisoserine increased only slightly (23 and 42%, respectively) over those of their full-length versions, largely because of improved turnover rates (Table 3). Guided by the slightly better catalytic efficiency of Phe-AT over Phe-AT(S563A) for phenylisoserine, we selected the former for the substrate specificity assays with various isoserine analogues.

Stereospecificity of Phe-AT for Phenylisoserine Stereoisomers. Earlier structure–activity relationship studies show that the natural (2R,3S)-phenylisoserine side chain isomer at C-13 of paclitaxel is important for its activity.^{22,42} A computational study that identified electronic and quantum features that defined bioactive molecules predicted that the (2S,3R)-stereoisomer in a paclitaxel variant was ~4-fold more effective than natural paclitaxel.⁴³ It should be noted that no empirical biological assays have been reported to date that verify this theoretical finding. Thus, here we explored the stereospecificity of Phe-AT, by separately incubating substrates (2R,3S)-, (2R,3R)-, or (2S,3R)-phenylisoserine with CoA, Mg²⁺, and ATP at apparent saturation. The (2S,3S)-isomer is in principle

Table 4. Biosynthesis of Isoleucine Analogues

$$22a - bb \xrightarrow{i^a} \begin{array}{c} \oplus \text{NH}_3 \\ | \\ \text{R}_1 - \text{CH} \\ | \\ \text{OH} \\ | \\ \text{C} = \text{O} \\ | \\ \text{SCoA} \end{array}$$

27a – bb

$\text{R}_1 =$ 27a (7.3 ± 0.91) (100%) ^b	 27b (0.98 ± 0.12) (14%)	 27c (6.1 ± 0.41) (84%)	 27d (4.0 ± 1.0) (55%)	 27e (0.11 ± 0.02) (2%)	 27f (1.7 ± 0.27) (24%)	 27g (0.45 ± 0.12) (6%)
 27h ND	 27i (1.4 ± 0.15) (19%)	 27j (0.22 ± 0.05) (3%)	 27k ND	 27l (2.6 ± 0.15) (36%)	 27m (1.1 ± 0.019) (15%)	 27n ND
 27o (0.6 ± 0.07) (8.2%)	 27p ND (0.044)	 27q (0.18 ± 0.02) (3%)	 27r (5.2 ± 0.10) (72%)	 27s (0.05 ± 0.01) (<1%)	 27t (0.3 ± 0.03) (4%)	 27u (0.04 ± 0.01) (<1%)
 27v ND (0.004)	 27w ND	 27x ND	 27y (0.9 ± 0.09) (12%)	 27z ND	 27aa ND	 27bb (0.09 ± 0.01) (1%)

^a(i) Mg²⁺ (3 mM), ATP (1 mM), CoA (1 mM), Phe-AT (1 mg), **22** (1 mM), pH 8.0, 31 °C, 2 h. ^bThe entries in parentheses in groups of two are apparent velocity (v_{app} in nanomoles per hour) and v_{rel} as a percentage with respect to **27a** from left to right, respectively. The v_{app} values of Phe-AT(W227S) are shown in bold and italics for **27p** and **27v**. ND indicates the biosynthetic product was below the detection limit of the mass spectrometer.

commercially available from specialized sources; however, it was cost prohibitive to obtain this isomer through custom synthesis at the time of this study. Our formidable efforts to synthesize the rare isomer fell beyond the scope of this study. The phenylisoserinyl CoA products were detected by electrospray ionization mass spectrometry (ESI-MS). Phe-AT turned over the (2*R*,3*S*)-isomer, having the same stereochemistry of the natural side chain of paclitaxel, 2-fold faster than it did the (2*R*,3*R*)-diastereomer. Under the same assay conditions, the CoA thioester of (2*S*,3*R*)-phenylisoserine was below the limits of detection (Table 3).

Relative Rates of Phe-AT for Isoleucine Substrate Analogues. In this study, the substrate scope of Phe-AT was assessed with racemic isoleucine substrates synthesized via the Staudinger reaction. Therefore, we estimated the magnitude and mode of inhibition on Phe-AT by the nonproductive (2*S*,3*R*)-enantiomer. In the presence of (2*S*,3*R*)-phenylisoserine at 250 μM , the $k_{\text{cat}}^{\text{app}}$ of Phe-AT for (2*R*,3*S*)-phenylisoserine was 0.12 min^{-1} , and the K_{M} was 500 μM , which was nearly identical to the K_{M} (440 μM) of Phe-AT in the absence of the inhibitor (Figure S41). The $k_{\text{cat}}^{\text{app}}$, however, decreased 15-fold from 1.51 min^{-1} , and the K_{I} was calculated to be 92.0 μM . The results indicated noncompetitive inhibition of Phe-AT by the nonproductive (2*S*,3*R*)-phenylisoserine enantiomer, suggesting that the enantiomer bound allosterically and affected turnover. These results showed that obtaining accurate apparent Michaelis parameters for each racemic isoleucine substrate tested herein was in part confounded by cosubstrate inhibition. Thus, the approximate relative steady-state rate of Phe-AT for each racemic isoleucine substrate was estimated through analysis of the biosynthesized isoleucine CoA by quantitative ESI-MS-MRM.

All substrates in which the phenyl ring had an *ortho*-(F, Cl, NO₂), *para*-(F, Cl, Br, CH₃, OH, NO₂), or *meta*-(F, Cl, Br,

CH₃, OH, CH₃O, NO₂) substituent were converted to their acyl CoA by Phe-AT. The enzyme activity was also observed with the nonaromatic β -(cyclohexyl)isoleucine and heteroaromatic β -(thiophenyl)isoleucine analogues, but not with the isopropyl- and *tert*-butylisoleucines or (pyridyl)isoleucine analogues (Table 4). The rate (7 nmol h^{-1}) at which Phe-AT converted phenylisoserine (prepared as a racemate) to its CoA thioester was set at 100% and used for comparison against the relative rates of Phe-AT for the other racemic isoleucine substrates at apparent saturation (1 mM) (Table 4).

In general, the v_{app} values of Phe-AT for substrates with *meta* substituents on the aryl ring were higher than those for the *para* and *ortho* isomers (Figure 3). For example, the v_{app} was \sim 1.5- and 6-fold lower for *p*- and *o*-fluoro isomers, respectively, than for the *m*-fluoro isomer. Similarly, the v_{app} for the methyl substituent on the phenyl ring of the isoleucine substrate was lower for the *o*-methyl (v_{app} below the detection limit) and *p*-methyl ($v_{\text{app}} = 1.13 \text{ nmol h}^{-1}$) isomers than for the *m*-methyl substrate ($v_{\text{app}} = 2.61 \text{ nmol h}^{-1}$) (Table 4). A model of Phe-AT was built using gramicidin synthetase A [Protein Data Bank (PDB) entry 1AMU] in complex with phenylalanine as the reference. We added chloro group(s) to the docked substrate to serve as representative substituent(s) for the other regioisomeric substrates used herein and to help identify the steric interactions that may affect turnover (Figure 3).

The model showed that residue Trp227 (i.e., W227) of Phe-AT is near (\sim 3.6 Å) the *para* carbon of the aryl ring of the substrate (Figure 3A). Thus, a rationale for the slower turnover of the *para*-substituted than of the *meta*-substituted substrates is steric compression between the *para* substituents and W227, preventing the latter from adopting a productive catalytic conformation (Figure 3B). By contrast, *meta* substituents likely avoid the more encumbered space near Ala224 and Phe566 and occupy an active site space closest to residues Ile318 and

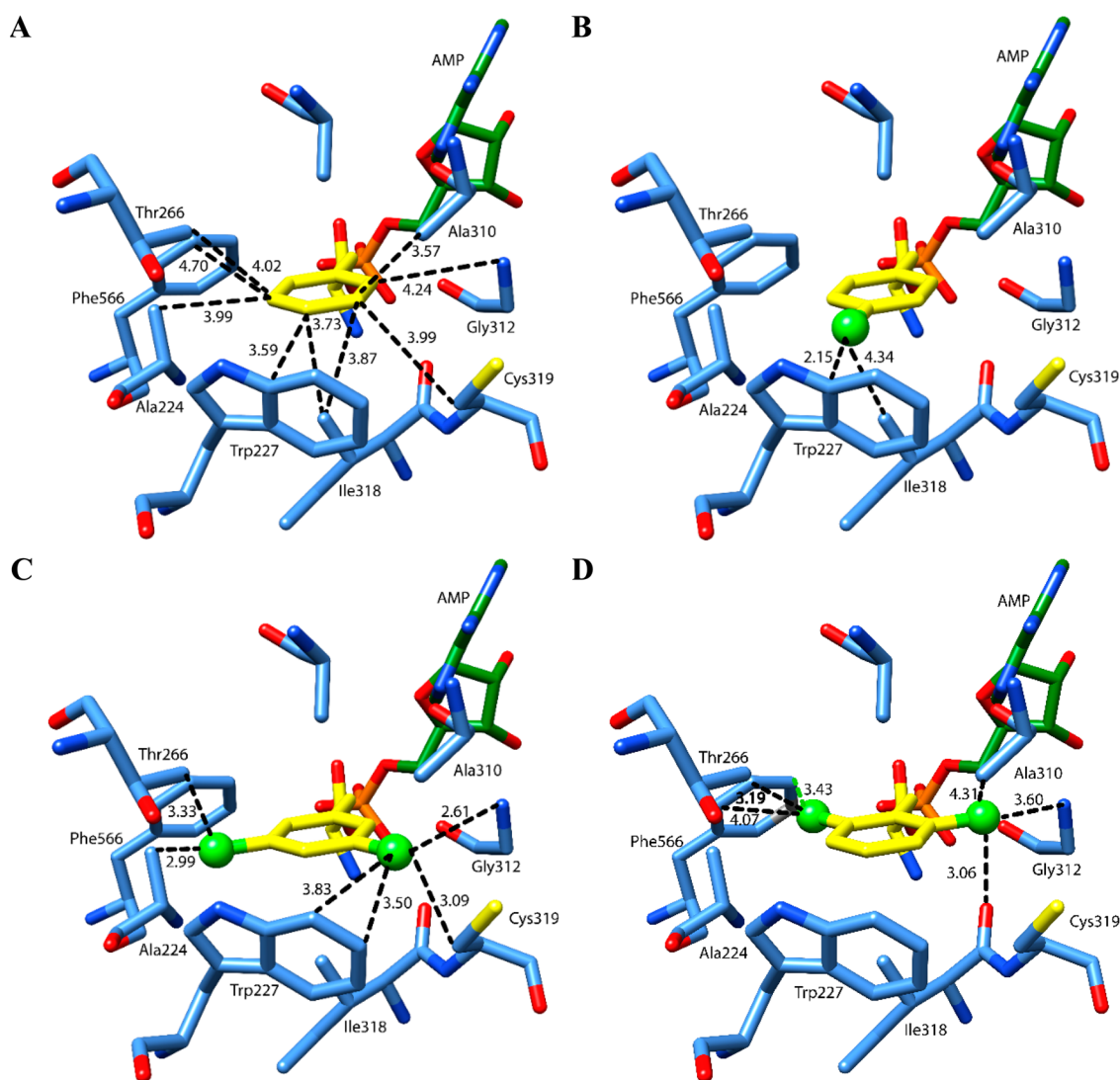


Figure 3. (A) Model of the Phe-AT active site built from gramicidin synthetase A (PDB entry 1AMU) in complex with phenylalanine. Shown are the AMP structure (green) and residues (lighter blue) within ~ 5 Å of the ring of the α -phenylalanine (yellow) complex. We used a chloro group as a representative substituent because its nominal van der Waals radius lies between those of second-row (C, O, and F) and fourth-row (Br) atoms of the various substituents in the substrates used here. Chloro substituents (green spheres) are added to the aryl ring of the docked substrate at the (B) *para*, (C) *meta*, and (D) *ortho* positions. The latter two positional isomers are shown as disubstituted to capture the steric interactions of both rotameric forms of the monosubstituted *meta* and *ortho* isomers used in this study. The chloro substituent also provides a good approximation of steric compression between the various substituents and nearby active site residues based on relative distance. Numbers next to dotted lines indicate distances of ≤ 4.70 Å; amino acid residues are listed as their three-letter codes followed by their position. Heteroatoms are nitrogen (darker blue), oxygen (red), sulfur (yellow), and phosphorus (orange).

Cys319 (Figure 3C). In the latter orientation, the *meta* substituent is estimated to be closest to the carbonyl oxygen of Gly312 (Figure 3C), but it should be noted that there is enough leeway for the phenyl ring to twist from its depicted plane to relieve steric interactions. In addition, we estimate from the model that *ortho* substituents are sterically compressed by Phe566 and likely are positioned closer to the carbonyl of Gly312 and the side chain of Ala310, and away from the carbonyl of Ile318 (Figure 3D). While this open cavity may provide sufficient space for the *ortho* substituents to reside, the substituents can still interact intramolecularly with the propanoate side chain of the substrate. This intramolecular interaction likely affects catalytic turnover by disrupting the motion of the propanoate during the carboxylate adenylation and thiolation reactions, as suggested for a homologous benzoyl CoA ligase in a recent study.⁴⁴

The v_{app} values of Phe-AT also correlated with the size of the halogen substituent, regardless of the position on the phenyl ring. This trend is demonstrated by substrates with the smaller fluoro substituent being converted fastest to their CoA thioesters in the halogen series: *o*-F > *o*-Cl > *o*-Br ($v_{app} = 0.98, 0.11, \text{ and } 0.0 \text{ nmol h}^{-1}$, respectively), *p*-F > *p*-Cl > *p*-Br ($v_{app} = 3.98, 0.45, \text{ and } 0.22 \text{ nmol h}^{-1}$, respectively), and *m*-F > *m*-Cl > *m*-Br ($v_{app} = 6.1, 1.7, \text{ and } 1.4 \text{ nmol h}^{-1}$, respectively). It is worth noting that the activity of Phe-AT with *m*- and *p*-Cl isoserinyl isomers is potentially prophetic toward making a (3,4-dichloro)phenylisoserinyl analogue of paclitaxel. The latter was shown in an earlier study to have microtubule assembly activity 7-fold greater than and melanoma cytotoxicity 40-fold greater than that of paclitaxel.⁴⁵

In general, the steric bulk of the substituent negatively affected turnover likely because of their inability to bind Phe-

AT in a catalytically competent conformation. The v_{app} for the production of the isoserinyl CoA analogues by Phe-AT decreased with an increasing size of the *para* substituent ($H > F > Cl > Br > OH \sim NO_2 > OCH_3$), ranging from 3.98 nmol h^{-1} for *p*-fluoro to a v_{app} that was below the detection limit of the mass spectrometer for the *p*-methoxy analogue. Among the heteroaromatic isoserine analogues, only thiophen-2-ylisoserine was converted to its CoA thioester by Phe-AT at a v_{app} of 0.89 nmol h^{-1} . Phe-AT did not turn over the pyridylisoserine isomers or the branched alkyl isopropyl- and *tert*-butylisoserine analogues to their CoA thioesters.

Expanding the Substrate Scope of Phe-AT for (Pyridyl)isoserines (27v, 27w, and 27x) and *p*-Methoxyphenylisoserine (27p). We were intrigued that the N heteroatom, bioisostere of carbon, prevented turnover of the pyridylisoserines by Phe-AT to their CoA thioesters. We imagine the pyridyl nitrogen likely H-bonds through an unknown bond network in the active site, placing the substrate in a nonproductive trajectory for catalysis. While a structural model of Phe-AT in complex with phenylalanine places W227 closest to the *para* position of the aryl ring of the substrate (Figure 3), the model also showed that second-shell Phe residues (F201, F202, and F206) border W227. The trifecta of Phe residues likely aligns W227 for favorable π -stacking with the substrate. Thus, W227 of Phe-AT was mutated alone or in tandem with the second-tier Phe triad. The triad was replaced by positionally equivalent residues found to occur naturally in homologous enzymes in an attempt to broaden the substrate specificity. W227 of Phe-AT was exchanged separately with polar residue Ser [labeled as Phe-AT(W227S)] that could potentially H-bond with the heteroatom of the pyridyl substrates. A different mutant, Phe-AT(W227A), was imagined to weaken steric interactions between the substituent on the substrate and the active site. F201 and F202 of Phe-AT(W227S) were also mutated to A201 and Q202, respectively [designated Phe-AT(W227S) (AQF)], to match the sequence of a nonribosomal peptide synthetase from *Anabaena* species (accession number D5J708) with a serine residue positioned like W227 in Phe-AT. In addition, F201, F202, and F206 of Phe-AT(W227A) were changed to A201, R202, and Y206, respectively [designated Phe-AT(W227A) (ARY)], to match the sequence of an amino acid adenylation enzyme from *Methylomicrobium album* BG8 (accession number H8GJ90) with an alanine residue positioned like W227 in Phe-AT.

We found that the solubly expressed Phe-AT(W227S) mutant slowly catalyzed the conversion of 2-pyridylisoserine to its CoA thioester (27v) ($v_{app} \sim 0.004$ nmol h^{-1}) but was not active with 3- or 4-pyridylisoserine. The latter CoAs were below the limits of detection. This turnover is a promising first-principles result for further development of the Phe-AT mutant to potentially make 3-fluoro-2-pyridylisoserinyl CoA for semibiosynthesis of the pharmaceutical tasetaxel⁴⁶ (see Table 1). Moreover, Phe-AT(W227S) turned over the sterically demanding *p*-methoxyphenylisoserine substrate to its thioester (27p), which was not made by Phe-AT (Table 3). Likely, the W227S replacement relieved the steric crowding near the *para* carbon of the substrate, allowing turnover of the larger substrate. We also determined that mutants Phe-AT(W227A), Phe-AT(W227S) (AQF), and Phe-AT(W227A) (ARY) did not turn over 2-, 3-, or 4-pyridylisoserine or *p*-methoxyphenylisoserine to its CoA thioester. The reason for the latter observations is unknown at this time.

In general, Phe-AT has similar relaxed substrate specificity as observed for other biocatalysts on the pathways of specialized natural products.^{47–55} This is a desirable feature in synthetic biology upon selection of biocatalysts to engineer a biosynthetic pathway that can recognize surrogate substrates. Phe-AT has significant potential to biosynthesize an array of aminoacyl CoAs that can be used by different acyl CoA-dependent acyltransferases to construct rare bioactive natural product analogues. In particular, Phe-AT has application for the design of a biosynthetic route to produce paclitaxel analogues that contain modified isoserine side chains. There are few bona fide CoA ligases identified that can activate an amino acid to its CoA thioester.⁵⁶ A query of “nonribosomal peptide synthetase” on the NCBI database captures ~ 200000 entries,⁵⁷ with each synthetase containing multiple AT domains that transiently thioesterify amino acids or polypeptides.⁵⁸ Repurposing the Phe-AT didomain of TycA as a CoA ligase suggests that other tandem AT domains of different NRPS enzymes may catalyze similar ligase activity. In addition, Phe-AT is a prime candidate for protein engineering through directed evolution^{59,60} with a goal of increasing its specificity and turnover profile, for example, for pyridylisoserine substrates to make oral forms of taxane drugs, such as tasetaxel. This would broaden the catalytic space of NRPS-loading modules to include an area where they can biosynthesize nonnatural acyl CoAs. It is imagined that the resulting thioesters can be used potentially by broad specificity CoA-dependent transferases to acylate and thus diversify bioactive specialized metabolites isolated from various other species.

■ ASSOCIATED CONTENT

📄 Supporting Information

The Supporting Information is available free of charge on the ACS Publications website at DOI: 10.1021/acs.biochem.6b01188.

Experimental methods, LC–MS/MS, kinetics, and NMR data (PDF)

■ AUTHOR INFORMATION

Corresponding Author

*E-mail: walker@chemistry.msu.edu.

ORCID

Kevin D. Walker: 0000-0001-5208-6692

Funding

The authors are grateful to the Michigan State University Office for Inclusion and Intercultural Initiatives for supporting the MSU Chemistry 4-Plus Bridge to the Doctorate Program (GA017081-CIEG) and for Michigan State University AgBioResearch Grant RA078692-894.

Notes

The authors declare no competing financial interest.

■ ACKNOWLEDGMENTS

The authors thank undergraduate Aaron Barto for his technical assistance.

■ REFERENCES

- (1) Bringi, V., Kadkade, P. G., L., P. C., and Roach, B. L. (Phyton Holdings, LLC) (2013) Enhanced production of Taxol and taxanes by cell cultures of *Taxus* species. U.S. Patent Appl. 20130017582.
- (2) Expósito, O., Bonfill, M., Moyano, E., Onrubia, M., Mirjalili, M. H., Cusidó, R. M., and Palazón, J. (2009) Biotechnological production

- of taxol and related taxoids: Current state and prospects. *Anti-Cancer Agents Med. Chem.* 9, 109–121.
- (3) Baloglu, E., and Kingston, D. G. I. (1999) The taxane diterpenoids. *J. Nat. Prod.* 62, 1448–1472.
- (4) Winkelnkemper, T., Schuldt, S., and Schembecker, G. (2011) Systematic downstream process development for purification of baccatin III with key performance indicators. *Sep. Purif. Technol.* 77, 355–366.
- (5) Walker, K., Fujisaki, S., Long, R., and Croteau, R. (2002) Molecular cloning and heterologous expression of the C-13 phenylpropanoid side chain-CoA acyltransferase that functions in Taxol biosynthesis. *Proc. Natl. Acad. Sci. U. S. A.* 99, 12715–12720.
- (6) Muchiri, R., and Walker, K. D. (2012) Taxol biosynthesis: Tyrocidine synthetase A catalyzes the production of phenylisoserinyl CoA and other amino phenylpropanoyl thioesters. *Chem. Biol.* 19, 679–685.
- (7) Jennewein, S., and Croteau, R. (2001) Taxol: biosynthesis, molecular genetics, and biotechnological applications. *Appl. Microbiol. Biotechnol.* 57, 13–19.
- (8) Jennewein, S., Wildung, M. R., Chau, M., Walker, K., and Croteau, R. (2004) Random sequencing of an induced *Taxus* cell cDNA library for identification of clones involved in Taxol biosynthesis. *Proc. Natl. Acad. Sci. U. S. A.* 101, 9149–9154.
- (9) Walker, K., Long, R., and Croteau, R. (2002) The final acylation step in Taxol biosynthesis: Cloning of the taxoid C13-side-chain *N*-benzoyltransferase from *Taxus*. *Proc. Natl. Acad. Sci. U. S. A.* 99, 9166–9171.
- (10) Khanna, C., Rosenberg, M., and Vail, D. M. (2015) A review of paclitaxel and novel formulations including those suitable for use in dogs. *J. Vet. Intern. Med.* 29, 1006–1012.
- (11) Rosenfield, K., Jaff, M. R., White, C. J., Rocha-Singh, K., Mena-Hurtado, C., Metzger, D. C., Brodmann, M., Pilger, E., Zeller, T., Krishnan, P., Gammon, R., Müller-Hülsbeck, S., Nehler, M. R., Benenati, J. F., and Scheinert, D. (2015) Trial of a paclitaxel-coated balloon for femoropopliteal artery disease. *N. Engl. J. Med.* 373, 145–153.
- (12) Pleva, L., Kukla, P., Kusnierova, P., Zapletalova, J., and Hlinomaz, O. (2016) Comparison of the efficacy of paclitaxel-eluting balloon catheters and everolimus-eluting stents in the treatment of coronary in-stent restenosis: The treatment of in-stent restenosis study. *Circ.: Cardiovasc. Interventions* 9, e004304.
- (13) Patil, Y., Sadhukha, T., Ma, L., and Panyam, J. (2009) Nanoparticle-mediated simultaneous and targeted delivery of paclitaxel and tariquidar overcomes tumor drug resistance. *J. Controlled Release* 136, 21–29.
- (14) Ojima, I., Chen, J., Sun, L., Borella, C. P., Wang, T., Miller, M. L., Lin, S., Geng, X., Kuznetsova, L., Qu, C., et al. (2008) Design, synthesis, and biological evaluation of new-generation taxoids. *J. Med. Chem.* 51, 3203–3221.
- (15) Dubois, J. (2006) Recent progress in the development of docetaxel and paclitaxel analogues. *Expert Opin. Ther. Pat.* 16, 1481–1496.
- (16) Ishiyama, T., Iimura, S., Yoshino, T., Chiba, J., Uoto, K., Terasawa, H., and Soga, T. (2002) New highly active taxoids from 9 β -dihydrobaccatin-9,10-acetals. Part 2. *Bioorg. Med. Chem. Lett.* 12, 2815–2819.
- (17) Takeda, Y., Uoto, K., Chiba, J., Horiuchi, T., Iwahana, M., Atsumi, R., Ono, C., Terasawa, H., and Soga, T. (2003) New highly active taxoids from 9 β -dihydrobaccatin-9,10-acetals. Part 4. *Bioorg. Med. Chem.* 11, 4431–4447.
- (18) Ojima, I., Duclos, O., Kuduk, S. D., Sun, C.-M., Slater, J. C., Lavelle, F., Veith, J. M., and Bernacki, R. J. (1994) Synthesis and biological activity of 3'-alkyl- and 3'-alkenyl-3'-dephenyldocetaxels. *Bioorg. Med. Chem. Lett.* 4, 2631–2634.
- (19) Georg, G. I., Cheruvallath, Z. S., Himes, R. H., Mejillano, M. R., and Burke, C. T. (1992) Synthesis of biologically active taxol analogs with modified phenylisoserine side chains. *J. Med. Chem.* 35, 4230–4237.
- (20) Georg, G. I., Cheruvallath, Z. S., Himes, R. H., and Mejillano, M. R. (1992) Semisynthesis and biological activity of taxol analogues: baccatin III 13-(*N*-benzoyl-(2'*R*,3'*S*)-3'-(*p*-tolyl)isoserinate), baccatin III 13-(*N*-(*p*-toluoyl)-2'*R*,3'*S*)-3'-phenylisoserinate), baccatin III 13-(*N*-benzoyl-(2'*R*,3'*S*)-3'-(*p*-trifluoromethylphenyl)isoserinate), and baccatin III 13-(*N*-(*p*-trifluoromethylbenzoyl)-(2'*R*,3'*S*)-3'-phenylisoserinate). *Bioorg. Med. Chem. Lett.* 2, 1751–1754.
- (21) Kingston, D. (2005) Taxol and Its Analogs. In *Anticancer Agents from Natural Products* (Cragg, G. M., Kingston, D., and Newman, D. J., Eds.) p 600, CRC Press, Boca Raton, FL.
- (22) Jiménez-Barbero, J., Souto, A. A., Abal, M., Barasoain, I., Evangelio, J. A., Acuña, A. U., Andreu, J. M., and Amat-Guerri, F. (1998) Effect of 2'-OH acetylation on the bioactivity and conformation of 7-O-[*N*-(4'-fluoresceincarboxyl)-*L*-alanyl]taxol. A NMR-fluorescence microscopy study. *Bioorg. Med. Chem.* 6, 1857–1863.
- (23) Kant, J., Huang, S., Wong, H., Fairchild, C., Vyas, D., and Farina, V. (1993) Studies toward structure-activity relationships of Taxol®: synthesis and cytotoxicity of Taxol® analogues with C-2' modified phenylisoserine side chains. *Bioorg. Med. Chem. Lett.* 3, 2471–2474.
- (24) Qi, X., Lee, S.-H., Yoon, J., and Lee, Y.-S. (2003) Synthesis of novel taxoid analogue containing sulfur group on C-13 side-chain: 2'-deoxy-2'-epi-mercaptapaclitaxel. *Tetrahedron* 59, 7409–7412.
- (25) Sharma, S., Lagisetty, C., Poliks, B., Coates, R. M., Kingston, D. G. I., and Bane, S. (2013) Dissecting paclitaxel–microtubule association: Quantitative assessment of the 2'-OH group. *Biochemistry* 52, 2328–2336.
- (26) Liu, C., Schilling, J. K., Ravindra, R., Bane, S., and Kingston, D. G. I. (2004) Syntheses and bioactivities of macrocyclic paclitaxel bis-lactones. *Bioorg. Med. Chem.* 12, 6147–6161.
- (27) Lu, H.-F., Xie, C., Chang, J., Lin, G.-Q., and Sun, X. (2011) Synthesis, cytotoxicity, metabolic stability and pharmacokinetic evaluation of fluorinated docetaxel analogs. *Eur. J. Med. Chem.* 46, 1743–1748.
- (28) Saif, M., Sarantopoulos, J., Patnaik, A., Tolcher, A., Takimoto, C., and Beeram, M. (2011) Teseaxel, a new oral taxane, in combination with capecitabine: A phase I, dose-escalation study in patients with advanced solid tumors. *Cancer Chemother. Pharmacol.* 68, 1565–1573.
- (29) Jing, Y.-r., Zhou, W., Li, W.-l., Zhao, L.-x., and Wang, Y.-f. (2014) The synthesis of novel taxoids for oral administration. *Bioorg. Med. Chem.* 22, 194–203.
- (30) Butler, M. S. (2008) Natural products to drugs: Natural product-derived compounds in clinical trials. *Nat. Prod. Rep.* 25, 475–516.
- (31) Gintjee, T. J. J., Magh, A. S. H., and Bertoni, C. (2014) High-throughput screening in duchenne muscular dystrophy: From drug discovery to functional genomics. *Biology* 3, 752–780.
- (32) Ojima, I., Duclos, O., Zucco, M., Bissery, M.-C., Combeau, C., Vrignaud, P., Riou, J. F., and Lavelle, F. (1994) Synthesis and structure-activity relationships of new antitumor taxoids. Effects of cyclohexyl substitution at the C-3' and/or C-2 of Taxotere (docetaxel). *J. Med. Chem.* 37, 2602–2608.
- (33) Flores, J. P., and Saif, M. W. (2013) Novel oral taxane therapies: Recent Phase I results. *Clin. Invest.* 3, 333–341.
- (34) Roswell Park Cancer Institute and National Cancer Institute. BAY 59-8862 in treating patients with non-small cell lung cancer. <http://clinicaltrials.gov/show/NCT00004451>, National Library of Medicine, Bethesda, MD (accessed October 18, 2016).
- (35) Walker, K., and Croteau, R. (1999) Taxol biosynthesis: A review of some determinant steps. *Recent Adv. Phytochem.* 33, 31–50.
- (36) Linne, U., Schäfer, A., Stubbs, M. T., and Marahiel, M. A. (2007) Aminoacyl-coenzyme A synthesis catalyzed by adenylation domains. *FEBS Lett.* 581, 905–910.
- (37) Wuts, P. G. M., Gu, R. L., and Northuis, J. M. (2000) Synthesis of (2*R*,3*S*)-isobutyl phenylisoserinate, the Taxol® side chain, from ethyl benzoylacetate. *Tetrahedron: Asymmetry* 11, 2117–2123.
- (38) Choudary, B. M., Chowdari, N. S., Madhi, S., and Kantam, M. L. (2003) A trifunctional catalyst for one-pot synthesis of chiral diols via

Heck coupling–N-oxidation–asymmetric dihydroxylation: Application for the synthesis of diltiazem and taxol side chain. *J. Org. Chem.* 68, 1736–1746.

(39) Hamamoto, H., Mamedov, V. A., Kitamoto, M., Hayashi, N., and Tsuboi, S. (2000) Chemoenzymatic synthesis of the C-13 side chain of paclitaxel (Taxol) and docetaxel (Taxotere). *Tetrahedron: Asymmetry* 11, 4485–4497.

(40) Lopez, R., Sordo, T. L., Sordo, J. A., and Gonzalez, J. (1993) Torqueelectronic effect in the control of the stereoselectivity of ketene-imine cycloaddition reactions. *J. Org. Chem.* 58, 7036–7037.

(41) Alcaide, B., Almendros, P., Carrascosa, R., and Torres, M. R. (2010) Synthesis of a new class of C2-symmetrical biheteroaryls by ammonium cerium(IV) nitrate mediated dimerization of 2-(furan-3-yl)pyrroles. *Eur. J. Org. Chem.* 2010, 823–826.

(42) Kingston, D. G., Chaudhary, A. G., Chordia, M. D., Gharpure, M., Gunatilaka, A. L., Higgs, P. L., Rimoldi, J. M., Samala, L., Jagtap, P. G., Giannakakou, P., et al. (1998) Synthesis and biological evaluation of 2-acyl analogues of paclitaxel (Taxol). *J. Med. Chem.* 41, 3715–3726.

(43) Braga, S. F., and Galvão, D. S. (2003) A structure–activity study of Taxol, Taxotere, and derivatives using the Electronic Indices Methodology (EIM). *J. Chem. Inf. Comput. Sci.* 43, 699–706.

(44) Thornburg, C. K., Wortas-Strom, S., Nosrati, M., Geiger, J. H., and Walker, K. D. (2015) Kinetically and Crystallographically Guided Mutations of a Benzoate CoA Ligase (BadA) Elucidate Mechanism and Expand Substrate Permissivity. *Biochemistry* 54, 6230–6242.

(45) Georg, G. I., Cheruvallath, Z. S., Harriman, G. C. B., Hepperle, M., Park, H., and Himes, R. H. (1994) Synthesis and biology of substituted 3'-phenyl taxol analogues. *Bioorg. Med. Chem. Lett.* 4, 2331–2336.

(46) Baas, P., Szczesna, A., Albert, I., Milanowski, J., Juhasz, E., Sztancsik, Z., von Pawel, J., Oyama, R., and Burgers, S. (2008) Phase I/II study of a 3 weekly oral taxane (DJ-927) in patients with recurrent, advanced non-small cell lung cancer. *J. Thorac. Oncol.* 3, 745–750.

(47) Rix, U., Fischer, C., Remsing, L. L., and Rohr, J. (2002) Modification of post-PKS tailoring steps through combinatorial biosynthesis. *Nat. Prod. Rep.* 19, 542–580.

(48) Firn, R. D., and Jones, C. G. (2003) Natural products - a simple model to explain chemical diversity. *Nat. Prod. Rep.* 20, 382–391.

(49) Firn, R. D., and Jones, C. G. (2000) The evolution of secondary metabolism – a unifying model. *Mol. Microbiol.* 37, 989–994.

(50) Drauz, K., and Waldmann, H. (1995) *Enzyme catalysis in organic synthesis: A comprehensive handbook*, John Wiley & Sons, New York.

(51) Liese, A., Seelbach, K., and Wandrey, C. (2006) *Industrial biotransformations*, John Wiley & Sons, New York.

(52) Schmid, A., Dordick, J. S., Hauer, B., Kiener, A., Wubbolts, M., and Witholt, B. (2001) Industrial biocatalysis today and tomorrow. *Nature* 409, 258–268.

(53) Patel, R. N. (2000) *Stereoselective biocatalysis*, CRC Press, Boca Raton, FL.

(54) Hutchinson, C. R. (1999) Microbial polyketide synthases: More and more prolific. *Proc. Natl. Acad. Sci. U. S. A.* 96, 3336–3338.

(55) Knight, Z. A., Gonzalez, B., Feldman, M. E., Zunder, E. R., Goldenberg, D. D., Williams, O., Loewith, R., Stokoe, D., Balla, A., Toth, B., et al. (2006) A pharmacological map of the PI3-K family defines a role for p110 α in insulin signaling. *Cell* 125, 733–747.

(56) Ramirez-Estrada, K., Altabella, T., Onrubia, M., Moyano, E., Notredame, C., Osuna, L., Vanden Bossche, R., Goossens, A., Cusido, R. M., and Palazon, J. (2016) Transcript profiling of jasmonate-elicited *Taxus* cells reveals a β -phenylalanine-CoA ligase. *Plant Biotechnol. J.* 14, 85–96.

(57) O'Leary, N. A., Wright, M. W., Brister, J. R., Ciufu, S., Haddad, D., McVeigh, R., Rajput, B., Robbertse, B., Smith-White, B., Ako-Adjei, D., Astashyn, A., Badretidin, A., Bao, Y., Blinkova, O., Brover, V., Chetvernin, V., Choi, J., Cox, E., Ermolaeva, O., Farrell, C. M., Goldfarb, T., Gupta, T., Haft, D., Hatcher, E., Hlavina, W., Joardar, V. S., Kodali, V. K., Li, W., Maglott, D., Masterson, P., McGarvey, K. M., Murphy, M. R., O'Neill, K., Pujar, S., Rangwala, S. H., Rausch, D., Riddick, L. D., Schoch, C., Shkeda, A., Storz, S. S., Sun, H., Thibaud-Nissen, F., Tolstoy, I., Tully, R. E., Vatsan, A. R., Wallin, C., Webb, D.,

Wu, W., Landrum, M. J., Kimchi, A., Tatusova, T., DiCuccio, M., Kitts, P., Murphy, T. D., and Pruitt, K. D. (2016) Reference sequence (RefSeq) database at NCBI: current status, taxonomic expansion, and functional annotation. *Nucleic Acids Res.* 44, D733–D745.

(58) Gulick, A. M. (2016) Structural insight into the necessary conformational changes of modular nonribosomal peptide synthetases. *Curr. Opin. Chem. Biol.* 35, 89–96.

(59) Kowalsky, C. A., Klesmith, J. R., Stapleton, J. A., Kelly, V., Reichkitzer, N., and Whitehead, T. A. (2015) High-Resolution Sequence-Function Mapping of Full-Length Proteins. *PLoS One* 10, e0118193.

(60) Badran, A. H., and Liu, D. R. (2015) In vivo continuous directed evolution. *Curr. Opin. Chem. Biol.* 24, 1–10.

(61) Gasteiger, E., Gattiker, A., Hoogland, C., Ivanyi, I., Appel, R. D., and Bairoch, A. (2003) ExPASy: The proteomics server for in-depth protein knowledge and analysis. *Nucleic Acids Res.* 31, 3784–3788.

(62) Gill, S. C., and von Hippel, P. H. (1989) Calculation of protein extinction coefficients from amino acid sequence data. *Anal. Biochem.* 182, 319–326.